Simulation of Polymer Removal from a Powder Injection Molding Compact by Thermal Debinding

Y.C. LAM, YING SHENGJIE, S.C.M. YU, and K.C. TAM

Powder injection molding (PIM) is an important net-shape manufacturing process. Thermal debinding is a common methodology for the final removal of residual polymer from a PIM compact prior to sintering. This process is an intricate combination of evaporation, liquid and gas migration, pyrolysis of polymer, and heat transfer in porous media. A better understanding of thermal debinding could lead to optimization of the process to prevent the formation of defects. Simulation of the process based on an integrated mathematical model for mass and heat transfer in porous media is proposed. The mechanisms of mass transport, *i.e.*, liquid flow, gas flow, vapor diffusion, and convection, as well as the phase transitions of polymer, and their interactions, are included in the model. The macroscopic partial differential equations are formulated by volume averaging of the microscopic conservation laws. The basic equations consist of mass conservation and energy conservation and are solved numerically. Polymer residue, pressure, and temperature distributions are predicted. The importance of the various mass transfer mechanisms is evaluated. The effects of key mass transfer parameters on thermal debinding are discussed. It is revealed from the results that the assumed binder front, which is supposed to recede into the powder compact as removal progresses, does not exist. The mass flux of polymer liquid is of the same order of the mass flux of polymer vapor in the gas phase, and the polymer vapor diffusion in the liquid phase is negligible.

I. INTRODUCTION

POWDER injection molding (PIM) is an important net-shape manufacturing process and has received much attention. One of the most critical steps in PIM process is debinding. It consumes a major part of the processing time. Failure of the powder compact often results if the process is accelerated. Thermal debinding is a common methodology for the final removal of residual polymer from a PIM compact prior to sintering. During debinding, polymer is heated thermally, melted into liquid, and decomposed into vapor. The overall removal of residual polymer is an intricate combination of evaporation, liquid and gas migration, pyrolysis of polymer, and heat transfer in porous media. A successful modeling of thermal debinding provides the potential for optimization of the process to prevent the formation of defects during the decomposition of the polymer. As summarized in Table I, several researchers attempted to model thermal debinding by considering various mass transport mechanisms.[1–9]

German[1] modeled isothermal debinding by two separate controlling processes: vapor diffusion and vapor permeation. The pyrolysis of binder and the diffusion of organic species within the binder phase, as well as the liquid transport processes, were neglected. The binder-vapor interface was modeled as a planar front, which receded into the compact as removal progressed. The effects of particle size, porosity, and component size on debinding times were assessed. Tsai[5] analyzed the gas pressure buildup and the stresses on the powder skeleton during binder burnout based on gas transport in a porous medium combining with the pyrolysis of binder and elasticity theory. Evans *et al.*[6] modeled the removal of polymer from molded ceramic bodies as an unsteady-state diffusion of degradation products in solution in the parent polymer and with degradation of polymer, and they evaluated the critical heating rates for the initial stage of polymer removal process. Mater *et al.*[7] further developed the work of Evans *et al.* and assumed that there was an undegraded shrinking core (or planar liquid-gas interface front) that receded into the compact as removal progressed so that the model would be applied not only for the initial stage of polymer removal process. Their model was extended to include gas transport in the porous outer layer of the compact. Lewis and Galler[8] applied the Monte-Carlo method to investigate the diffusion of volatile species in the binder phase and the capillary-driven binder redistribution processes in the isothermal removal of plasticizer species. Barone and Ulciny[3] studied the capillary-driven liquid flow during the removal of organic binders from injection-molded ceramic components. They neglected the gas transport phenomenon and deemed that the liquid-phase transport processes dominate throughout most of the debinding cycle. Stangle and Aksay[4] modeled thermal debinding by considering the liquid phase transport and gas phase transport in porous media and analyzed the internal stresses generated during binder removal.

Hitherto, one or two mass transfer mechanisms were considered to be dominant during the debinding processes and others were ignored. As some mass transfer mechanisms and their interaction, which might be important to binder removal, were ignored, the predicted results were not exactly reliable. For example, experimental evidence indicated that the assumption of planar binder front (or planar binder-vapor interface) did not reflect the physical reality of thermal debinding. Cima and Lewis reported the development of a nonplanar pore front (or binder-vapor interface) as removal

Y.C. LAM, S.C.M. YU, and K.C. TAM, Associate Professors, and YING SHENGJIE, Research Fellow, are with the School of Mechanical and Production Engineering, Nanyang Technological University, Singapore 639798.

Manuscript submitted November 29, 1999.

Table I. Modeling of Thermal Debinding Process

References	Comments
German[1]	vapor diffusion in porous media, vapor permeation in porous media
Calver and Cima[2]	vapor diffusion in polymer liquid + vapor diffusion in porous outer layer
Barone and Ulicny[3]	capillary-driven liquid flow in porous media
Stangle and Aksay[4]	liquid and gas flow in porous media
Tsai[5]	vapor permeation in porous media
Evans *et al.*[6]	vapor diffusion in polymer liquid
Mater *et al.*[7]	vapor diffusion in polyer liquid + vapor permeation in porous outer layer
Lewis and Galler[8]	vapor diffusion in polymer liquid and liquid redistribution
Maximenko and Biest[9]	vapor diffusion and liquid flow in porous media

progressed during thermal debinding[10] and directly observed such processes in two-dimensional binder-filled pore networks.[11] The calculated times[2] taken for the binder to burn out were overestimated and the predicted critical heating rates[6,7,9] were underestimated. Most of the existing work considered two mass transport mechanisms, *i.e.*, polymer vapor diffusion in the polymer liquid[2,6–9] and gas flow.[1,4,5] Some work[3,4] emphasized liquid flow. During the final removal of residual polymer from a PIM compact by thermal debinding, however, existing investigations did not provide a clear understanding on the interaction of various mass transfer mechanisms and on the role played by the individual mass transfer mechanism. Thus, the major objective of this investigation is to gain some understanding on the role played by the various mechanisms of polymer removal.

The present investigation adopts an integrated approach in that the mechanisms of mass transfer, *i.e.*, liquid and gas flows, vapor diffusion, and convection, as well as the phase transitions of solid into liquid and liquid into vapor are considered simultaneously. A numerical algorithm is developed to solve the control equations. The polymer residue, pressure, and temperature distributions in the compact during thermal debinding are evaluated and analyzed. The effects of key mass transfer parameters on thermal debinding are discussed. The simulated results indicated that the polymer removal is mainly controlled by the degradation of the polymer. The assumed binder front (or liquid-vapor interface), which is supposed to recede into the powder compact as removal progresses, does not exist. The polymer liquid flux is of the same order of the polymer vapor flux in the gas phase, and the polymer vapor diffusion in the liquid phase is negligible. The initial opened porosity is conducive to reducing the internal pressure of the compact to prevent the formation of defects.

II. MATHEMATICAL MODEL

To capture the physics of the problem without unnecessary complication, a one-dimensional problem, *i.e.*, a flat-plate shape PIM compact, is considered. Consistent with current technology, other components of the binder system, *e.g.*, wax and stearic acid, are assumed to have been removed by wicking debinding or solvent extraction prior to thermal debinding. During debinding, polymer is heated thermally, melted into liquid, decomposed into vapor, and removed from the outer surface of the compact. The effect of the deformation of the powder skeleton on mass and heat transfer is ignored. One surface of the compact (the outer surface) is exposed to an atmospheric air flux. The other surface

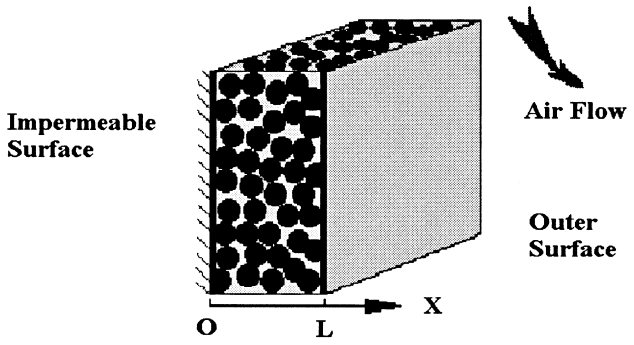

Fig. 1—Geometrical model.

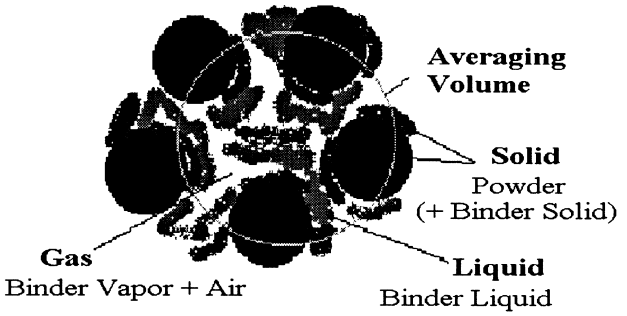

Fig. 2—Macroscopic model.

(the impermeable surface) is considered to be adiabatic and impermeable, which could be a plane of symmetry, (Figure 1).

The macroscopic partial differential equations can be achieved by volume averaging of the microscopic conservation laws. Over the averaging volume *V*, as shown in Figure 2, three types of averages can be defined, according to Whitaker.[12] First, the spatial average of a physical quantity Ω of species *i* is defined by

$$\langle \Omega^i \rangle = \frac{1}{V} \int_v \Omega^i dV \qquad [1]$$

Second, the phase average of the phase *j* (*j* = *s*, *l*, and *g*, representing solid, liquid, and gas phases, respectively) is defined by

$$\langle \Omega^j \rangle = \frac{1}{V} \int_v \Omega^j dV \qquad [2]$$

Third, the intrinsic phase average is defined by

$$\langle \Omega^i \rangle_j = \frac{1}{V^j} \int_{V^j} \Omega^i dV \quad [3]$$

It is noted that

$$V = V^s + V^l + V^g \quad [4]$$

where V^s, V^l, and V^g are the volumes of solid, liquid, and gas phases, respectively. We define the volume fractions of solid, liquid, and gas phases as

$$n^s = \frac{V^s}{V}, \quad n^l = \frac{V^l}{V}, \quad n^g = \frac{V^g}{V} \quad [5]$$

These volume fractions must sum to unity:

$$n^s + n^l + n^g = 1 \quad [6]$$

If we define the porosity of compact as δ, then

$$\delta = 1 - n^s = n^l + n^g \quad [7]$$

In this analysis, the Dalton partial pressure[13] is adopted, therefore,

$$n^g = n^{ag} = n^{bg} = \delta - n^l \quad [8]$$

where superscripts *ag* and *bg* represent atmospheric air and polymer (binder) vapor, respectively. The intrinsic phase average and spatial average are related by

$$\langle \Omega \rangle = n^j \langle \Omega \rangle_j \quad [9]$$

For the polymer, the mass conservation equations of solid, liquid and vapor can be written as

$$\frac{\partial \langle \rho^{bs} \rangle}{\partial t} = -\langle m_{ls} \rangle \quad [10]$$

$$\frac{\partial \langle \rho^{bl} \rangle}{\partial t} + \frac{\partial \langle J^{bl} \rangle}{\partial x} = \langle m_{ls} \rangle - \langle m_{gl} \rangle \quad [11]$$

and

$$\frac{\partial \langle \rho^{bg} \rangle}{\partial t} + \frac{\partial \langle J^{bg} \rangle}{\partial x} = \langle m_{gl} \rangle \quad [12]$$

where ρ^{bs}, ρ^{bl}, and ρ^{bg} are the densities of polymer (binder) solid, liquid, and vapor, respectively, J^{bl} and J^{bg} are the mass fluxes of polymer liquid and vapor, respectively; and m_{ls} and m_{gl} are the rates of mass transformation of polymer solid into liquid and liquid into vapor, respectively. Equations [10] through [12] can be combined to yield

$$\frac{\partial \langle R^b \rangle}{\partial t} + \frac{\partial \langle J^b \rangle}{\partial x} = 0 \quad [13]$$

where R^b is the polymer (binder) residue:

$$\langle R^b \rangle = \langle \rho^{bs} \rangle + \langle \rho^{bl} \rangle + \langle \rho^{bg} \rangle \quad [14]$$

and J^b is the net polymer (binder) mass flux, equal to the liquid flux plus the vapor flux:

$$\langle J^b \rangle = \langle J^{bl} \rangle + \langle J^{bg} \rangle \quad [15]$$

The polymer liquid flux can be written as[12]

$$\langle J^{bl} \rangle = \rho^{bl} \langle \mathbf{v}^l \rangle \quad [16]$$

where $\mathbf{v}^l$ is the velocity of the liquid phase.

The polymer vapor flux consists of the vapor flux in the gas phase and in the liquid phase:

$$\langle J^{bg} \rangle = \langle J_g^{bg} \rangle + \langle J_l^{bg} \rangle \quad [17]$$

To distinguish between the vapor concentration in the gas phase and in the liquid phase, the local chemical thermodynamic equilibrium is assumed and the partitioning concept[14] is adopted:

$$\langle \rho_l^{bg} \rangle = \langle \chi \rho_g^{bg} \rangle \quad [18]$$

$$\langle \rho^{bg} \rangle = \langle \rho_g^{bg} \rangle + \langle \rho_l^{bg} \rangle \quad [19]$$

where χ is the interaction parameter for polymer liquid and vapor system, which can be determined from Henry's law constant and solubility relation.

The polymer vapor flux in the gas phase can be expressed as[12]

$$\langle J_g^{bg} \rangle = \left\langle \frac{\rho^{bg}}{1 + \chi} \right\rangle_g \langle \mathbf{v}^g \rangle - \langle \rho^g \rangle_g D_{\text{eff}}^{bgg} \frac{\partial}{\partial x} \left(\left\langle \frac{\rho^{bg}}{1 + \chi} \right\rangle_g / \langle \rho^g \rangle_g \right) \quad [20]$$

where $\mathbf{v}^g$ is the velocity of the gas phase and D_{eff}^{bgg} is the coefficient of the effective diffusion of polymer vapor and atmospheric air in a porous medium. The first term of the right-hand side of Eq. [20] represents vapor convection with gas flow, and the second term represents vapor diffusion in the gas phase.

The polymer vapor flux in the liquid phase, representing the movement of the solute of polymer degradation products in the solution of polymer liquid, which includes the convection and diffusion contributions,[15] can be expressed as

$$\langle J_l^{bg} \rangle = \left\langle \frac{\chi \rho^{bg}}{1 + \chi} \right\rangle \langle \mathbf{v}^l \rangle - D_{\text{eff}}^{bgl} \frac{\partial \left\langle \frac{\chi \rho^{bg}}{1 + \chi} \right\rangle}{\partial x} \quad [21]$$

where D_{eff}^{bgl} is the coefficient of the effective diffusion of polymer vapor in the polymer liquid. The first term of the right-hand side of Eq. [21] represents vapor convection with liquid flow, and the second term represents vapor diffusion in the liquid phase.

The velocities of the fluid are obtained using Darcy's law. Gravitational effect is ignored. For the liquid phase,

$$\langle \mathbf{v}^l \rangle = -\frac{KK^l}{\mu^l} \frac{\partial}{\partial x} (\langle p^g \rangle_g - p_c) \quad [22]$$

where p^g and p_c are the gas and capillary pressures, respectively. The terms K and K^l are the intrinsic and relative permeability, respectively, of the liquid phase; and μ^l is the dynamic viscosity of the liquid phase. For the gas phase, Darcy's law can be written as

$$\langle \mathbf{v}^g \rangle = -\frac{KK^g}{\mu^g} \frac{\partial \langle p^g \rangle_g}{\partial x} \quad [23]$$

where K^g is the relative permeability of the gas phase and μ^g is the dynamic viscosity of the gas phase.

To consider the effect of atmospheric air, the mass conservation of atmospheric air can be written as[12]

$$\frac{\partial \langle \rho^{ag} \rangle}{\partial t} + \frac{\partial}{\partial x} (\langle \rho^{ag} \rangle_g \langle \mathbf{v}^{ag} \rangle) = 0 \quad [24]$$

where

$$\langle \rho^{ag} \rangle_g \langle \mathbf{v}^{ag} \rangle = \langle \rho^{ag} \rangle_g \langle \mathbf{v}^g \rangle - \langle \rho^g \rangle_g D_{\text{eff}}^{bgg} \frac{\partial}{\partial x} (\langle \rho^{ag} \rangle_g / \langle \rho^g \rangle_g) \quad [25]$$

The gas phase is assumed to be an ideal mixture of perfect gases; then,

$$\langle p^{bg}\rangle_g = \langle \rho^{bg}\rangle_g \, \mathrm{R}\langle T\rangle / M^{bg} \quad [26]$$

$$\langle p^{ag}\rangle_g = \langle \rho^{ag}\rangle_g \, \mathrm{R}\langle T\rangle / M^{ag} \quad [27]$$

and

$$\langle p^{g}\rangle_g = \langle p^{bg}\rangle_g + \langle p^{ag}\rangle_g \quad [28]$$

where M^{bg} and M^{ag} are the molar masses of polymer (binder) vapor and atmospheric air, T is the absolute temperature, and R is the universal gas constant.

Form the Flory–Huggins equation,[16] the polymer vapor pressure can be expressed as

$$\langle p^{bg}\rangle_g = p_0^{bg} \frac{n^{bg}}{\delta} \exp\left[\frac{n^{bl}}{\delta} + \chi\left(\frac{n^{bl}}{\delta}\right)^2\right] \quad [29]$$

where p_0^{bg} is the polymer vapor pressure over the pure polymer liquid and can be estimated using the well-known Clausius–Clapeyron equation

$$\ln p_0^{bg} = -\frac{\Delta H_{\mathrm{vap}}}{\mathrm{R}T} + I \quad [30]$$

where ΔH_{vap} is the enthalpy of polymer vaporization and I is a constant.

The intrinsic kinetics of polymer thermal degradation is usually studied using thermal gravimetric analysis (TGA).[17] The shape of the pyrolysis curve with powder is similar to that without powder. Therefore, the mathematical form of polymer thermal degradation is still applicable:

$$\langle m_{gl}\rangle = \langle \rho^{bl}\rangle K_0 \exp\left(-\frac{E}{\mathrm{R}T}\right) \quad [31]$$

where K_0 and E are the specific rate constant and activation energy, respectively, for thermal degradation. These can be obtained from TGA data on a thin film sample or a sample of the order of a hundred milligrams, where there are no transport limitations.

The energy conservation equation can be expressed in the form

$$\frac{\partial}{\partial x}\left(\langle k_{\mathrm{eff}}\rangle \frac{\partial\langle T\rangle}{\partial x}\right) - \langle \rho^l c^l \mathbf{v}^l + \rho^g c^g \mathbf{v}^g\rangle \frac{\partial\langle T\rangle}{\partial x} + \langle \tilde{Q}\rangle = \langle \rho c\rangle \frac{\partial\langle T\rangle}{\partial t} \quad [32]$$

where k_{eff} is the effective thermal conductivity and c is the specific heat. Depending on temperature, $\tilde{Q}$ is either the rate of heat generated by polymer phase transition from solid to liquid or from liquid to vapor. The second term on the left-hand side of Eq. [32] represents the convective heat flux caused by the liquid and gas flow.

The solution of the system equations required initial and boundary conditions. Initially, the temperature of the compact is constant, *i.e.*, room temperature. The initial opened porosity is filled with atmospheric air and its pressure is equal to the ambient pressure. During thermal debinding, on the impermeable surface ($x = 0$), the heat and mass fluxes are null. On the outer surface ($x = L$), the total gas pressure is equal to the ambient pressure. The polymer liquid flux is equal to zero (as no liquid 'pumping' is assumed), and the surface evaporation of the polymer liquid is governed by Eq. [31]. The prescribed surface temperature condition is adopted, which is a good approximation for low heating rate.

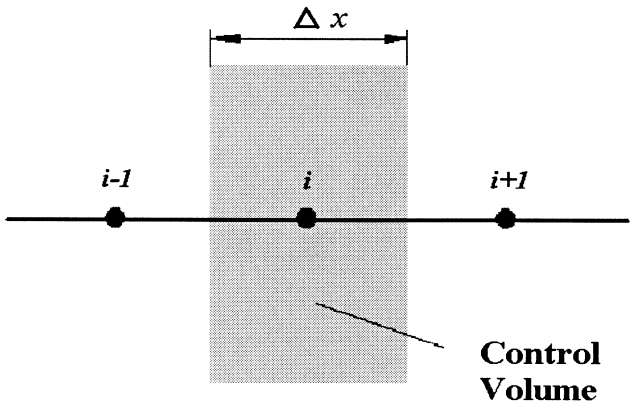

Fig. 3—Control domain of discretization.

III. NUMERICAL SOLUTION

The finite difference numerical scheme based on the notion of control domain as described by Patankar[18] is adopted. The domain of integration constitutes a grid of points i around which are control volumes (Figure 3). On the surfaces of the compact, half the control domain is considered and the boundary conditions are imposed. A computer code is developed to simulate the thermal debinding process numerically.

To illustrate the proposed model and numerical scheme, carbonyl iron is chosen as the metal powder. The polymer component in the binder system is chosen to be polyalphamethylstyrene, as it degrades exclusively to monomer during thermolysis, and the data required for the modeling of the degradation and diffusion are available. It is assumed that the powder loading is 0.6 volume fraction and the polymer volume fraction of the binder system is 0.5. The other components of the binder system are assumed to have been removed by wicking debinding or solvent extraction prior to thermal debinding. The distance between the impermeable surface and the outer surface of the compact is 5 mm. The atmospheric air is nitrogen, the ambient pressure is atmospheric, and the heating rate is 1 K/min during thermal debinding. The physical characteristics and the appropriate equations with the relevant constants are detailed in the Appendix.

IV. RESULTS AND DISCUSSIONS

Figure 4 shows the total polymer binder residue (remained polymer mass divided by original polymer mass of the entire compact) curve during thermal debinding. Before the polymer degrades, the rate of polymer removal is very low. The rate of polymer removal increases rapidly as the temperature reaches 290 °C (4.5 hours), which is within the decomposition temperature range of the polymer. After the binder residue decreases to 0.18, which corresponds to the irreducible liquid saturation of 0.09 (the polymer fraction in the binder system is assumed to be 0.5; thus, the polymer binder residue is approximately double that of the polymer liquid saturation), the rate of polymer removal becomes slow.

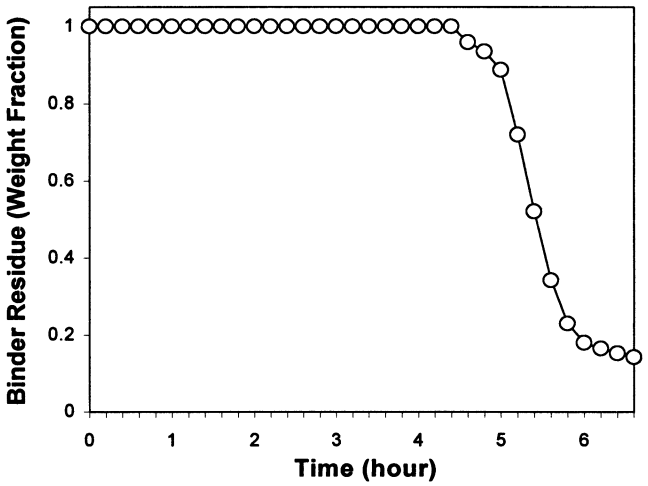

Fig. 4—Total polymer residue *vs* time.

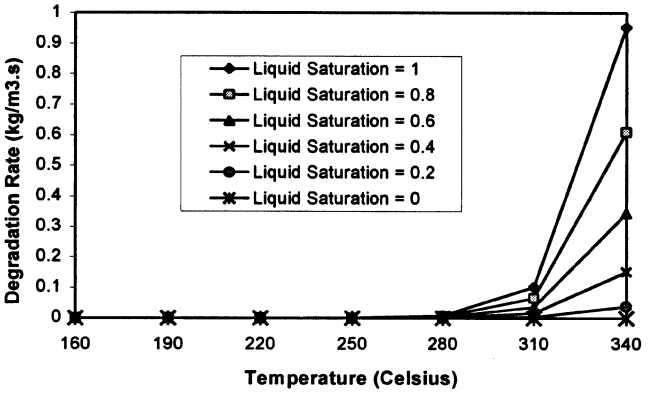

Fig. 5—Polymer degradation rate *vs* temperature.

Figure 5 shows the polyalphamethylstyrene polymer degradation rate curves calculated using Eq. [31]. The polymer degradation rate is very low until the temperature reaches about 280 °C. Subsequently, the polymer degradation rate increases rapidly with an increase in temperature. The polymer degradation rate also increases with an increase in polymer liquid saturation. Comparing with the total polymer residue curve Figure 4, it is revealed that the polymer removal process is mainly controlled by polymer degradation during thermal debinding. The temperature at which significant removal of polymer in the compact occurs is slightly retarded (at 290 °C in Figure 4 compared to 280 °C in Figure 5) because of the resistance to mass transport by a porous medium.

Figure 6 shows the polymer binder residue (remained polymer mass divided by original polymer mass) distribution as a function of distance from the impermeable surface. A prerequisite assumption of some researchers[1,2,7] is that there exists a distinct liquid-gas interface, that recedes into the compact as removal progresses. The present analysis indicates that such a distinct interface does not exist. There is a continuous change of liquid concentration along the distance from the impermeable surface, and it is in agreement with the experimental surveys of Barone *et al.*[19]

As shown as Figure 6, at the initial stage of polymer removal, the polymer residue distribution is almost uniform.

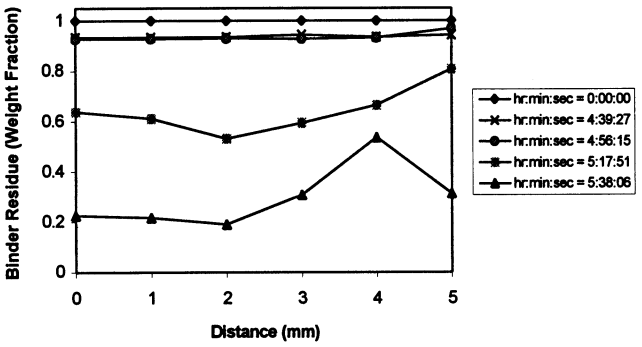

Fig. 6—Polymer binder residue *vs* distance.

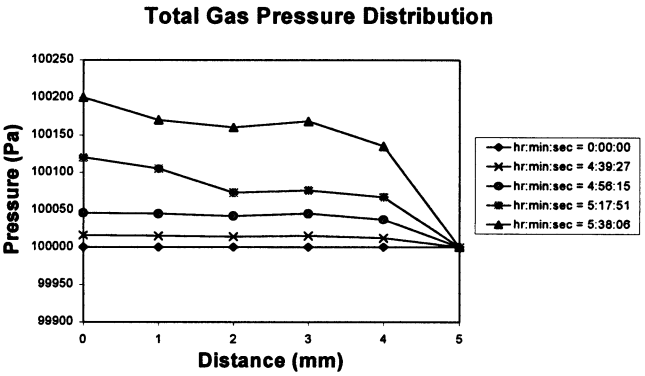

Fig. 7—Total gas pressure *vs* distance.

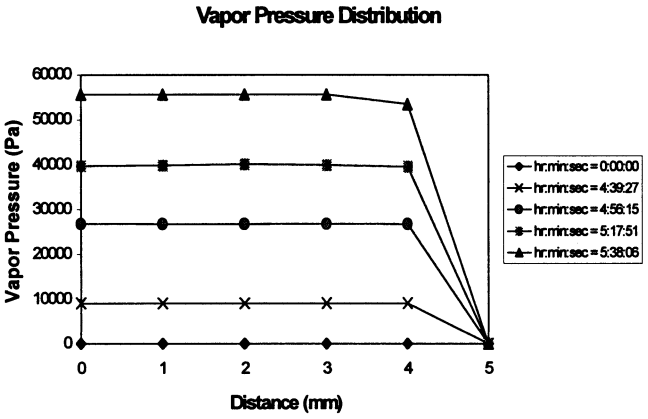

Fig. 8—Polymer vapor pressure *vs* distance.

There is little accumulation of polymer at the outer surface of the compact because the polymer liquid is driven to flow to the outer surface by gas pressure. At the later stage of polymer removal, the peak accumulation of polymer retreats a little from the outer surface of the compact because the rate of polymer evaporation at the outer surface increases rapidly. As the removal process progresses, the difference between the concentration of polymer at the outer surface and the internal regions increases, with the outer surface region having a higher concentration. This prediction is in agreement with the experimental observations of Sproson and Messing,[20] Su,[21] and Hwang and Tsou.[22] This phenomenon is caused by an increase in total gas pressure at the internal of the compact, as shown in Figure 7.

Figure 8 shows the polymer vapor pressure distribution

curves. The polymer vapor pressure increases rapidly with an increase of the accumulation of polymer vapor generated by polymer degradation in the internal of the compact. It is important to control the polymer degradation rate to prevent excessive internal pressure, which is the key cause of compact failure during thermal debinding.

Table II shows the orders of magnitude of the maximum values of various mass transfer quantities during the final removal of residual polymer from a PIM compact by thermal debinding. It can be observed that the average gas velocity is of the order of 10^{-3} to 10^{-4} m/s, four orders of magnitude greater than the average liquid velocity 10^{-7} to 10^{-8} m/s. However, as the polymer liquid density is much greater than the polymer vapor density, when liquid flow happens, the average polymer liquid mass flux is of the same order of the average polymer vapor mass flux in the gas phase. But the average polymer vapor mass flux in the liquid phase is only of the order of 10^{-7} to 10^{-8} kg/m^2 · s, four orders of magnitude less than the average polymer vapor flux in the gas phase, 10^{-3} to 10^{-4} kg/ m^2 · s. The average polymer vapor diffusion in the liquid phase is of the order of 10^{-15} to 10^{-16} kg/m^2 · s, which is negligible compared to the average polymer vapor flux in the liquid phase, 10^{-7} to 10^{-8} kg/m^2 · s. It is clear that the existing models, which are based mainly on polymer vapor diffusion in the polymer liquid,[2,6–9] are not suitable for modeling the final removal of residual polymer from a PIM compact by thermal debinding.

There are three escape routes for the polymer. First, polymer liquid is driven to flow from the internal of the compact to the outer surface by pressures, and then it evaporates from the outer surface of the compact. Second, polymer degrades into vapor in the internal of the compact and the polymer vapor flows from the internal to the outer surface of the compact through convection and diffusion in the gas phase and is subsequently removed by the atmospheric air stream. Third, the polymer vapor that is dissolved in the polymer liquid flows from the internal to the outer surface of the compact because of convection and diffusion with the polymer liquid, and then it is removed by the atmospheric air stream.

Until the polymer liquid saturation decreases to the irreducible liquid saturation (0.09), the polymer liquid flow and the polymer vapor flow of the gas phase dominate the polymer removal process. Subsequently, the polymer liquid flow can no longer occur, and the polymer removal process is dominated by the polymer vapor flow in the gas phase. The polymer vapor flow in the polymer liquid phase is negligible, as shown by comparing it with the polymer vapor flow of the gas phase and the polymer liquid flow. Thus, models in which gas flow is only considered[1,5] or liquid flow is only considered[3] are not adequate to model the final removal of residual polymer from a PIM compact by thermal debinding.

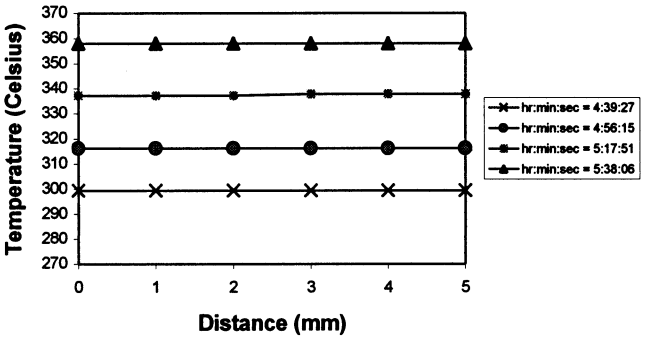

Fig. 9—Temperature *vs* distance.

Figure 9 shows the temperature distribution curves during polymer removal. The temperature distribution is almost uniform, and the differences of temperature in the internal of the compact are of the order of 10^{-1} to 10^{-2} °C. This is expected, as the heating rate of the thermal debinding process is slow and the thickness of the compact is thin. The temperature distribution is also related to the thermal properties of the constituent phases, the heat effects of pyrolysis, and the convective heat flow due to liquid and gas flow. The polymer degradation rate and its accompanying heat generation rate are normally kept low to prevent the generation of a large amount of vapor, a key origin of unfavorable internal stress in the powder skeleton. Similarly, since the liquid and gas flow rates are usually small, their convective contribution is also small.

The flow of polymer liquid is driven by polymer capillary pressure and gas pressure. Figure 10 shows the polyalphamethylstyrene polymer capillary pressure curves calculated

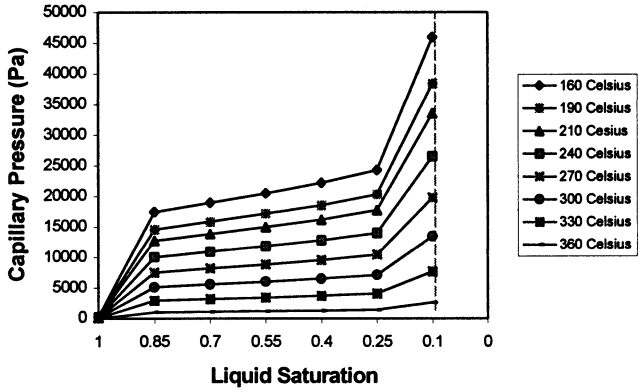

Fig. 10—Polymer capillary pressure *vs* liquid saturation.

Table II. Orders of Magnitude of the Maximum Values of Various Mass Transfer Quantities

Mass Transfer Quantity	Order of Magnitude
Average liquid velocity (m/s)	10^{-7} to 10^{-8}
Average gas velocity (m/s)	10^{-3} to 10^{-4}
Average polymer liquid flux (kg/m^2 · s)	10^{-3} to 10^{-5}
Average polymer vapor flux in the gas phase (kg/m^2 · s)	10^{-3} to 10^{-4}
Average polymer vapor flux in the liquid phase (kg/m^2 · s)	10^{-7} to 10^{-8}
Average polymer vapor diffusion in the liquid phase (kg/m^2 · s)	10^{-15} to 10^{-16}

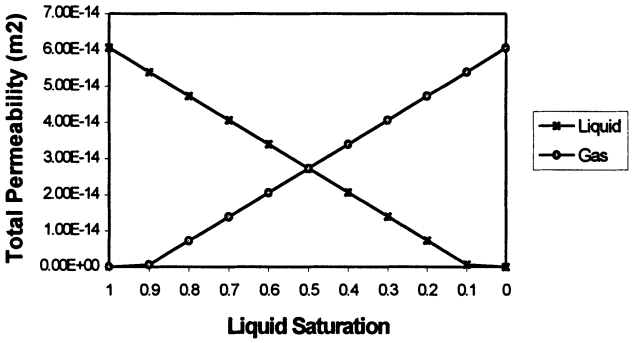

Fig. 11—Total permeability *vs* liquid saturation.

using Eq. [A15]. The polymer capillary pressure increases with a decrease of polymer liquid saturation. The polymer capillary pressure decreases with an increase in temperature. The temperature distribution of the compact is almost uniform, as shown in Figure 9. There is negligible temperature difference within the compact. Thus, the capillary pressure differences caused by the temperature differences are small. During polymer removal, the capillary pressure differences are mainly caused by polymer liquid saturation differences, *i.e.*, the polymer residue differences. In other words, the capillary-driven liquid flow is controlled by the polymer residue differences. It drives the polymer liquid to flow from the point of higher polymer residue to the point of lower polymer residue. The polymer residue distribution shown in Figure 6 indicates that there is accumulation of polymer near the outer surface of the compact. This is caused by the higher gas pressure in the internal of the compact and the lower gas pressure in the outer surface of the compact (Figure 7). It is evident that the pressure-forced liquid flow controls liquid-phase transport and the capillary-driven liquid flow is minor. Thus, the model of capillary-driven liquid flow[3] alone is not suitable for the final removal of residual polymer from a PIM compact by thermal debinding.

Figure 11 shows the total permeability (intrinsic permeability multiplied by relative permeability) curves of liquid and gas calculated using Eqs. [A1] through [A5]. The total permeability of gas increases linearly and the total permeability of liquid decreases linearly with a decrease of liquid saturation. After the liquid saturation decreases to the irreducible liquid saturation (0.09), there is no more liquid flow. The polymer-wax based binder system normally contains one-third polymer. This means that the polymer liquid saturation is approximately in the range of 0 to 0.3 during the final removal of residual polymer from a PIM compact by thermal debinding. In the range of 0 to 0.3 liquid saturation, the total permeability of gas is greater than the total permeability of liquid. Furthermore, gas with lower viscosity tends to migrate more rapidly due to its low resistance to flow. Thus, lower liquid saturation is favorable to gas flow. However, the polymer degradation rate decreases with a decrease in polymer liquid saturation, as shown in Figure 5. When gas flow is sufficiently rapid to decrease the accumulation of polymer vapor in the internal of the compact, the vapor pressure could be reduced to avoid damaging the compact. Thus, the initial opened porosity is important for proper removal of polymer from a PIM compact. In other words, the polymer content of a binder system should be as low as possible but still meet the rheologic requirements for injection.

V. CONCLUSIONS

An integrated model for the various interactive effects of various mechanisms of polymer removal from a PIM compact by thermal debinding is proposed. The polymer residue distribution, pressure distribution, and temperature distribution can be predicted and the importance of the various removal mechanisms can be evaluated.

During the final removal of residual polymer from a PIM compact, the polymer removal process is mainly controlled by polymer thermal degradation. There are three main routes for the internal polymer escaping away from the compact. First, polymer liquid is driven to flow from the internal of the compact to the outer surface primarily by pressure-forced flow. It subsequently evaporates from the outer surface of the compact until the polymer liquid saturation decreases to the irreducible liquid saturation. Second, polymer degrades to vapor in the internal of the compact and the polymer vapor flows from the internal to the outer surface of the compact due to convection and diffusion in the gas phase. It is subsequently removed away by the atmospheric air stream. Third, the polymer vapor that dissolved in the polymer liquid flows from the internal to the outer surface of the compact because of convection with the polymer liquid flow and diffusion in the polymer liquid, and then it is removed by the atmospheric air stream. The third route is negligible in comparison to the first two routes.

The initial opened porosity is conducive to reducing the internal pressure of the compact to prevent defects from occurring during the final removal of residual polymer from a PIM compact by thermal debinding.

APPENDIX

Evaluating equations of coefficients and constants from the literatures

Intrinsic permeability:[23]

$$K = 4.8 \times 10^{-13}\, d^{1.3}\, (1 - \varepsilon_s)^{4.8} \qquad [A1]$$

where K is in square meters, d is the average diameter of powder particles in micrometers, and ε_s is the powder loading.

Carbonyl iron of $d = 6\ \mu$m is chosen.

Relative permeability of liquid phase:[24]

$$K^l = (S - S_{ir})/(1 - S_{ir}),\ S > S_{ir} = 0.09 \qquad [A2]$$

$$K^l = 0,\ S < S_{ir} \qquad [A3]$$

where S is the liquid saturation defined by $S = n^l/\delta$ and S_{ir} is the irreducible saturation that marks the onset of the pendular state when liquid transport can no longer occur.

Relative permeability of gas phase:

$$K^g = 1 - 1.1S,\ S < S'_{ir} = 1/1.1 \qquad [A4]$$

$$K^g = 0,\ S > S'_{ir} \qquad [A5]$$

Enthalpy of vaporization at normal boiling point:[25]

$$\Delta H_{\text{vap}b} = 1.093 RT_c \left(T_{br} \frac{\ln P_c - 1.013}{0.930 - T_{br}} \right) \qquad [A6]$$

where ΔH_{vapb} is in J/mol; P_c is the critical pressure in bar;, T_c and T_b are the critical temperature and normal boiling point, respectively, in Kelvin; and T_{br} is the reduced temperature at the normal boiling point, *i.e.*, $T_{br} = T_b/T_c$.

Alphamethylstyrene:[26] $P_c = 34$ bar, $T_c = 654$ K, and $T_b = 438.5$K.

Estimation of the enthalpy of vaporization at any temperature from a known value at a single temperature:[27]

$$\frac{\Delta H_{vap2}}{\Delta H_{vap1}} = \left(\frac{1 - T_{r2}}{1 - T_{r1}}\right)^{0.38} \quad [A7]$$

Dynamic viscosity of liquid phase:[28]

$$\ln \mu^l = A + \frac{B}{T + C} \quad [A8]$$

where μ^l is in Pa · s, T is in Kelvin, A is a dimensionless constant, and B and C are constants (in Kelvin).
Polyalphamethylstyrene:[6] $A = -7.355$, $B = 494.9$ K, and $C = -107$ K.

Dynamic viscosity of gas phase:[26]

$$\mu^g = \frac{26.69(MT)^{1/2}}{a^2\Omega_v} \quad [A9]$$

where μ^g is in μP; M is in g/mol; T is in Kelvin; a is the molecular diameter in Angstrom,

$$a = 0.809\ V_c^{1/3} \quad [A10]$$

where V_c is the critical volume in cm^3 /mol; and Ω_v is the collision integral[29]

$$\Omega_v = A\,(T^*)^{-B} + C[\exp(-DT^*)] + E[\exp(-FT^*)] \quad [A11]$$

where $A = 1.16145$, $B = 0.14874$, $C = 0.52487$, $D = 0.77320$, $E = 2.16178$, $F = 2.43787$, and $T^* = \varkappa T/\varepsilon$, with ε being the characteristic energy in Joule and $\varkappa$ the Boltzmann's constant in J/K,

$$\frac{\varepsilon}{\varkappa} = 1.15T_b \quad [A12]$$

where $\varepsilon/\varkappa$ and T_b are in Kelvin.

Alphamethylstyrene:[26] $M = 118.179$ g/mol and $V_c = 108$ cm^3/mol.

Nitrogen:[26] $M = 28.013$ g/mol, $V_c = 89.8$ cm^3/mol, and $T_b = 77.4$ K.

Dynamic viscosity of gas mixture:[30]

$$\mu^g = \sum_{i=1}^{n} \frac{y_i\mu_i^g}{\sum_{j=1}^{n} y_i\phi_{ij}} \quad [A13]$$

where μ^g and μ_i^g are in μP, y_i is the pure component mole fraction, and

$$\phi_{ij} = \frac{[1 + (\mu_i^g/\mu_j^g)^{1/2}\,(M_i/M_j)^{1/4}]^2}{[8(1 + M_i/M_j)]^{1/2}} \quad [A14]$$

where M is in g/mol.

Capillary pressure:[24]

$$p_c = \left(\frac{\delta}{K}\right)^{1/2} \sigma J(S) \quad [A15]$$

where K is in square meters, and

$$J(S) = 0.364\{1 - \exp[-40(1 - S)]\} + 0.221(1 - S) + 0.005/(S - 0.09) \quad [A16]$$

and σ is the surface tension in N/m,[26]

$$\sigma = [P_c^{2/3}\,T_c^{1/3}\,Q(1 - T_r)^{11/9}] \times 10^{-3} \quad [A17]$$

and

$$Q = 0.1196\left[1 + \frac{T_{br}\ln(P_c/1.01325)}{1 - T_{br}}\right] - 0.279 \quad [A18]$$

where P_c is in bar, and T_c, T_b, and T are in Kelvin.

Diffusion coefficient for binary gas system:[29]

$$D = \frac{(3.03 - 0.98/M_{AB}^{1/2})T^{3/2} \times 10^{-3}}{pM_{AB}^{1/2}\,a_{AB}^2\Omega_D} \quad [A19]$$

where D is in cm^2/s, T is in Kelvin, p is in bar, and M is in g/mol,

$$M_{AB} = \frac{2M_AM_B}{M_A + M_B} \quad [A20]$$

and a is in Angstrom,

$$a_{AB} = \frac{a_A + a_B}{2} \quad [A21]$$

The term Ω_D is the dimensionless diffusion collision integral,

$$\Omega_D = \frac{A}{(T^*)^B} + \frac{C}{\exp(DT^*)} + \frac{E}{\exp(FT^*)} + \frac{G}{\exp(HT^*)} \quad [A22]$$

where $A = 1.06036$, $B = 0.15610$, $C = 0.19300$, $D = 0.47635$, $E = 1.03587$, $F = 1.52996$, $G = 1.76474$, $H = 3.89411$, and $T^* = \varkappa T/\varepsilon_{AB}$, where $\varkappa$ is in J/K, T is in Kelvin, and ε is in Joule,

$$\varepsilon_{AB} = (\varepsilon_A\varepsilon_B)^{1/2} \quad [A23]$$

Effective diffusivity:[31]

$$D_{eff} = D(1 - S)^2\,(n^g)^{4/3} \quad [A24]$$

Diffusion coefficient for polymer-monomer system:[32]

$$D = D_{01}\,(1 - \phi)^2(1 - 2\,\chi\phi)\exp\left\{\frac{-[W_1V_1(0) + W_2\xi V_2(0)]}{V_f/\omega}\right\} \quad [A25]$$

In addition,

$$D_{01} = D_0\exp\left(-\frac{E_D}{RT}\right) \quad [A26]$$

$$\phi = \frac{W_1V_1}{W_1V_1 + W_2V_2} \quad [A27]$$

and

$$\frac{V_f}{\omega} = \frac{\Phi_{11}}{\omega}\,W_1\,[(c_2)_1 + T - (T_g)_1] + \frac{\Phi_{12}}{\omega}\,W_2\,[(c_2)_2 + T - (T_g)_2] \quad [A28]$$

where D is in m^2/s, D_0 is the pre-exponential factor for

diffusion in m^2/s, E_D is the activation energy for diffusion in J/mol, R is in J/mol, T is in Kelvin, W_1 and W_2 are the weight fractions of monomer and polymer in the polymer-monomer system, V_1 and V_2 are the specific volumes of monomer and polymer in m^3/ kg, $V_1(0)$ and $V_2(0)$ are the specific volumes of monomer and polymer at 0 K, ω is the dimensionless overlap factor for free volume, ξ is the dimensionless ratio of critical molar volumes of hopping units of monomer and polymer, V_f is the average hole free volume per unit mass in m^3/kg, Φ_{11} and Φ_{12} are the free-volume parameters for monomer and polymer in m^3/kg, $(c_2)_1$ and $(c_2)_2$ are the Williamas–Landel–Ferry constants for monomer and polymer in Kelvin, and $(T_g)_1$ and $(T_g)_2$ are the glass transition temperatures for monomer and polymer in Kelvin.

Alphamethylstyrene:[6] $D_0 = 6.92 \times 10^{-4}$ m^2/s, $E_D =$ 38,370 J/mol, $\chi = 0.361$, $\xi = 0.54$, $\Phi_{11}/\omega = 1.756 \times 10^{-6} m^3/kg \cdot K$, $\Phi_{12}/\omega = 5.127 \times 10^{-7}$ $m^3/kg \cdot K$, $V_1(0) = 8.686 \times 10^{-4}$ m^3/kg, $V_2(0) = 7.975 \times 10^{-4}$ m^3/kg, $(c_2)_1 =$ 13.27K, $(c_2)_2 = 49.3K$, $(T_g)_1 = 120$ K, and $(T_g)_2 = 442$ K.

Effective diffusivity:[33]

$$D_{\text{eff}} = \frac{\delta S}{Z} D \qquad [A29]$$

where Z is the tortuosity,[34]

$$Z = \frac{1}{\delta} \qquad [A30]$$

Thermal degradation parameters of polyalphamethylstyrene:[6] specific rate constant for thermal degradation $K_0 = 1.67 \times 10^{16}$ 1/s; activation energy for thermal degradation $E = 222{,}000$ J/mol.

TABLE OF SYMBOLS

A	constant in Eqs. [A8], [A11], and [A22]
B	constant in Eq. [A8], K; constant in Eqs. [A11] and [A22]
c	specific heat, J/kg · K
$(c_2)_1$	Williamas–Landel–Ferry constants for monomer, K
$(c_2)_2$	Williamas–Landel–Ferry constants for polymer, K
C	constant in Eq. [A8], K; constant in Eqs. [A11] and [A22]
d	average diameter of powder particles, m, μm
D	diffusion coefficient, m^2/s, cm^2/s; constant in Eqs. [A11] and [A22]
D_0	pre-exponential factor for diffusion, m^2/s
E	activation energy for thermal degradation, J/mol; constant in Eqs. [A11] and [A22]
E_D	activation energy for diffusion, J/mol
F	constant in Eqs. [A11] and [A22]
G	constant in Eq. [A22]
H	constant in Eq. [A22]
ΔH_{vap}	enthalpy of vaporization, J/mol
I	constant in Eq. [30]
J	mass flux, $kg/m^2 \cdot s$
$J(S)$	J function defined by Eq. [A16]
k	thermal conductivity, W/m · K
K_0	specific rate constant for thermal degradation, 1/s
m	rate of mass alteration, $kg/m^3 \cdot s$
M	molar mass, kg/mol, g/mol
n	volume fraction
p	pressure, Pa
p_0^{bg}	polymer vapor pressure over pure polymer liquid, Pa
p_c	capillary pressure, Pa, bar (1 bar = 10^5 Pa)
P_c	critical pressure, Pa, bar (1 bar = 10^5 Pa)
$\tilde{Q}$	rate of heat generated by phase transition, $J/m^3 \cdot s$
R	universal gas constant, 8.314 J/mol · K
R^b	polymer (binder) residue, kg/m^3
S	liquid saturation
S_{ir}	irreducible liquid saturation for liquid flow
t	time, s
T	temperature, K
T_b	normal boiling point, K
T_c	critical temperature, K
T_r	reduced temperature
$(T_g)_1$	glass transition temperatures for monomer, K
$(T_g)_2$	glass transition temperatures for polymer, K
$\mathbf{v}$	velocity, m/s
V	volume, m^3
V_1	specific volumes of monomer, m^3/kg
$V_1(0)$	specific volumes of monomer at 0 K, m^3/kg
V_2	specific volumes of polymer, m^3/kg
$V_2(0)$	specific volumes of polymer at 0 K, m^3/kg
V_c	critical volume, m^3/mol, cm^3/mol
V_f	average hole free volume per unit mass, m^3/kg
W_1	weight fractions of monomer in polymer-monomer system
W_2	weight fractions of polymer in polymer-monomer system
x	coordinate, m
y_i	pure component mole fraction
Z	tortuosity
a	molecular diameter, Å (1 Å = 10^{-10} m)
δ	porosity, volume fraction
ε	characteristic energy, J
ε_s	powder loading, volume fraction
$\varkappa$	Boltzmann's constant, J/K
K	intrinsic permeability, m^2
K^g	relative permeability of gas phase
K^l	relative permeability of liquid phase
μ	dynamic viscosity, Pa · s, P (1 P = 0.1 Pa · s)
ξ	ratio of critical molar volumes of hopping units of monomer and polymer
ρ	density, kg/m^3
σ	surface tension, N/m
Φ_{11}	free-volume parameters for monomer, m^3/kg
Φ_{12}	free-volume parameters for polymer, m^3/kg
χ	interaction parameter for polymer liquid and vapor system
ω	overlap factor for free volume
Ω_D	diffusion collision integral defined by Eq. [A22]
Ω_v	collision integral defined by Eq. [A11]
$\langle\ \rangle$	volume averaging operator as defined in Eqs. [1]–[3]

Superscripts

ag	atmospheric air
bg	polymer (binder) vapor
bgg	polymer (binder) vapor in the gas phase
bgl	polymer (binder) vapor in the liquid phase
bl	polymer (binder) liquid
bs	polymer (binder) solid

g	gas phase
l	liquid phase
s	solid phase

Subscripts

eff	effective
g	gas phase
gl	phase transition of polymer from liquid into vapor
l	liquid phase
ls	phase transition of polymer from solid into liquid
s	solid phase

REFERENCES

1. R.M. German: *Int. J. Powder Metall.*, 1987, vol. 23 (4), pp. 237-45.
2. P. Calvert and M. Cima: *J. Am. Ceram. Soc.*, 1990, vol. 73 (3), pp. 575-79.
3. M.R. Barone and J.C. Ulicny: *J. Am. Ceram. Soc.*, 1990, vol. 73 (11), pp. 3323-33.
4. G.C. Stangle and I.A. Aksay: *Chem. Eng. Sci.*, 1990, vol. 45 (7), pp. 1719-31.
5. D.-S. Tsai: *AIChE J.*, 1991, vol. 37 (4), pp. 547-54.
6. J.R.G. Evans, M.J. Edirisinghe, J.K. Wright, and J. Crank: *Proc. R. Soc. London A*, 1991, vol. 432, pp. 321-40.
7. S.A. Mater, M.J. Edirisinghe, J.R.G. Evans, E.H. Twizell, and J.H. Song: *J. Mater. Sci.*, 1995, vol. 30, pp. 3805-10.
8. J.A. Lewis and M.A. Galler, *J. Am. Ceram. Soc.*, 1996, vol. 79 (5), pp. 1377-88.
9. A. Maximenko and O. Van Der Biest: *J. Eur. Ceram. Soc.*, 1998, vol. 18, pp. 1001-09.
10. M.J. Cima, J.A. Lewis, and A. Devoe: *J. Am. Ceram. Soc.*, 1989, vol. 72 (7), pp. 1192-99.
11. J.A. Lewis and M.J. Cima: in *Ceramic Transactions, Ceramic Powder Science III*, G.L. Messing, S. Hirano, and H. Hausner, eds., American Ceramic Society, Westerville, OH, 1990, vol. 12, pp. 583-90.
12. S. Whitaker: in *Advances in Heat Transfer*, Academic Press, New York, NY, 1977, vol. 13, pp. 119-203.
13. D.M. Himmelblau: *Basic Principles and Calculations in Chemical Engineering*, 5th ed. Simon & Schuster Pte Ltd., 1992.
14. C.Y. Wang and P. Cheng: *Int. J. Heat Mass Transfer*, 1996, vol. 39 (17), pp. 3607-18.
15. E.L. Cussler: *Diffusion: Mass Transfer in Fluid Systems*, Cambridge University Press, Cambridge, United Kingdom, 1984.
16. P.J. Flory: *Principles of Polymer Chemistry*, Cornell University Press, Ithaca, NY, 1953, pp. 495-540.
17. C.D. Doyle: in *Techniques and Methods of Polymer Evaluation*, vol. I. *Thermal Analysis*, P.E. Slade and L.T. Jenkins, eds., Edward Arnold, London 1966, pp. 113-234.
18. S.V. Patanker: *Numerical Heat Transfer and Fluid Flow*, Hemisphere Publishing Co., New York, NY, 1980.
19. M.R. Barone, J.C. Ulicny, R.R. Hengst, and J.P. Pollinger: in *Ceramic Transactions, Ceramic Powder Science II, A*, C.L. Messing, E.R. Fuller, and H. Hausner, Jr., eds., The American Ceramic Society, Westerville, OH, 1988, vol. 1, pp. 575-83.
20. D.W. Sproson and G.L. Messing: in *Ceramic Transactions, Ceramic Powder Science II, A*, C.L. Messing, E.R. Fuller, and H. Hausner, Jr., eds., The American Ceramic Society, Inc., Westerville, OH, 1988, vol. 1, pp. 528-37.
21. S.R. Su: *Synthesis and Processing of Ceramics: Scientific Issues*, Materials Research Society Symposia Proceedings, W.E. Rhine, T.M. Shaw, R.J. Cottschall, and Y. Chen, eds., Materials Research Society, Pittsburgh, PA, 1992, vol. 249, pp. 345-51.
22. K.S. Hwang and T.H. Tsou: *Metall. Trans. A*, 1992, vol. 23A, pp. 2775-82.
23. R.M. German: *Powder Technol.*, 1981, vol. 30, pp. 81-86.
24. A.E. Scheidegger: *The Physics of Flow through Porous Media*, 3rd ed., University of Toronto Press, Toronto, 1974.
25. L. Riedel: *Chem. Ing. Technol.*, 1954, vol. 26, p. 679.
26. R.C. Ried, J.M. Prausintz, and B.E. Poling: *The Properties of Gases & Liquids*, 4th ed., McGraw-Hill, Inc., New York, NY, 1987.
27. K.M. Watson: *Ind. Eng. Chem.*, 1943, vol. 35, p. 398.
28. H. Vogel: *Phys. Z.*, 1921, vol. 22, p. 645.
29. P.D. Neufeld, A.R. Janzen, and R.A. Aziz: *J. Chem. Phys.*, 1972, vol. 57, p. 1100.
30. C.R.J. Wilke: *Chem. Phys.*, 1950, vol. 18, p. 517.
31. L.D. Baver and W.H. Gardner: *Soil Physics*, 4th ed., Wiley, New York, NY, 1972.
32. J.L. Duda, J.S. Vrentas, S.T. Ju, and H.T. Liu: *AIChE J.*, 1982, vol. 28, pp. 279-85.
33. E.A. Mason, A.P. Malinauskas, and R.B. Evans: *J. Chem. Phys.*, 1967, vol. 46, pp. 3199-21.
34. N. Wakao and J.M. Smith: *Chem. Eng. Sci.*, 1962, vol. 17, pp. 825-34.